Journal of Sound and Vibration (1999) **228**(5), 995–1015
Article No. jsvi.1999.2439, available online at http://www.idealibrary.com on IDEAL®

THE EFFECT OF MULTIPLE IMPACTS ON THE DYNAMICS OF AN IMPACT SYSTEM

X. C. YIN AND L. G. WANG

Department of Applied Mechanics, Nanjing University of Science and Technology, Nanjing, 210014, *Peoples Republic of China*

(*Received* 14 *September* 1998, *and in final form* 9 *June* 1999)

The dynamics of an impact system of two concentric hollow cylinders with a clearance is investigated by using a continuous model and the theory of wave propagation. Exact solutions are obtained by the expansion of the transient wave function in a series of eigenfunctions, and their numerical results are presented by selecting a suitable number of truncation terms of eigenfunctions. The effect of multiple impact is considered. The impact clusters sensitive to the time step length, truncation terms of eigenfunctions and system parameters, are studied in comparison to single impacts. Two evolving ways of impact clusters are observed. The impact responses, frequency spectra and reconstructed phase portraits demonstrate complicated motions including quasi-periodic and chaotic motions, two routes to chaos through two-frequency quasi-periodicity and intermittency, phase locking and the low-dimensional behavior of the system. This investigation also verifies the validity of the simplified models for describing impact systems.

1. INTRODUCTION

In mechanisms and machines, impact oscillations result from components impacting each other due to the clearances of these mechanical systems. Impact vibration is of interest in a wide variety of engineering applications. The simplified models commonly used have been developed, based on Newton's law and impact law (Newton's law of restitution). The complicated vibro-impact responses show non-linear characterization in these models [1–5]. Periodic, subharmonic and low-dimensional chaotic motions have been found.

At least two questions arise when the simplified models are applied. One is the infinite degrees of freedom of continuous impacting bodies. The equation for solving the impact response should be a partial differential equation. Its phase space is infinite. Does such an infinite-dimensional system behave as a low-dimensional system or exhibit low-dimensional attractors? The other is due to the existence of multiple sub-impacts influence the dynamics of the system? Only a few studies of multiple sub-impacts have been conducted. Mason [6] showed that an impact that appeared single to the naked eye consisted in reality of several impacts in quick succession. These impacts can be called sub-impacts, which form an impact cluster. Stoianovici and Hurmuzlu [7] conducted an experiment of freely

0022-460X/99/500995 + 21 $30.00/0

dropped bars on a large external surface. The authors detected sub-impacts in a drop, checked Mason's notation and showed that the multiple sub-impacts caused the variation of the coefficient of restitution. Goldsmith [8] and Yigit *et al.* [9] have also made some remarks on multiple sub-impacts.

The problem of multiple sub-impacts is usually concerned with the continuous modes and transient deformations, and encounters serious difficulties in the mathematical treatment. However, two studies have been made for two simple impact systems by using the continuous models and considering the transient deformations [10, 11]. One system consists of two concentric hollow cylinders with a zero clearance in our previous work [10]. The other consists of a thin beam impacting against a stop [11]. The two studies gave some numerical results of impact forces and responses.

The present paper considers an axially symmetric plain strain problem for an impact system with a small non-zero clearance. The system (Figure 1) consists of two infinite, coaxial, hollow, circular, elastic cylinders. The two hollow cylinders initially at rest have perfectly smooth surfaces and same materials. There is a small clearance Δ between them. The interior hollow cylinder is subjected to an interior pressure $p_1(t)$ uniformly distributed along the axis. Once the dilation of the interior hollow cylinder grows to be equal to the value of the clearance, the interior hollow cylinder will start impacting against the outer hollow cylinder. Figure 1 is an idealization of the behaviour of a tube at a guide tube or a bushing. A liquid or a gas flows in the tube. The applied pressure $p_1(t)$ depends on the flow velocity. Sometimes the operations of opening and closing the system may cause impulsive pressure. High pressure may also be generated by explosive gas. The impact response of such an ordinary mechanical system is important in high-integrity designs. The dynamics of the impact system can be studied by the use of the continuous model and theory of wave propagation. Exact solutions and their numerical results can be obtained, showing multiple sub-impacts clearly. It provides us with a good example to study the effect of multiple sub-impacts on the dynamics of impact systems.

In this paper, the theory of wave propagation is applied. The corresponding partial differential equations are derived. Exact solutions are obtained by the expansion of the transient wave function in a series of eigenfunctions. Numerical results are presented by selecting 100–200 terms of eigenfunctions. A certain multiple impact phenomenon called the clustering phenomenon is examined, where

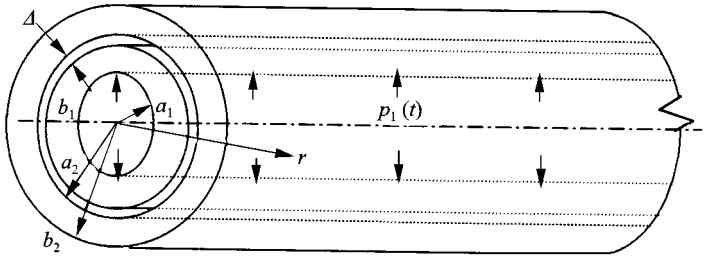

Figure 1. Geometry of the system with two hollow cylinders (initial state).

several single impacts take place closely together to form an impact cluster. The impact clusters are less sensitive to calculating errors than the single impacts. They may grow either regularly or irregularly. Two evolving ways are found. The dynamic behavior of the system is studied by impact responses, frequency spectra and reconstructed phase portraits. The investigation demonstrates the low-dimensional behavior of the system. The validity of the simplified models is discussed as well.

2. MATHEMATICAL FORMULATION

The sizes of the two hollow cylinders are shown in Figure 1. The interior hollow cylinder has inner and outer radii a_1 and b_1 respectively, and the outer hollow cylinder has inner and outer radii a_2 and b_2 respectively. The clearance Δ is much smaller than radius b_1. The two hollow cylinders have the same Lame's constants $\lambda = \mu = 80$ GPa, and longitudinal velocity $C = 5000$ m/s. To simulate impulsive pressure. $p_1(t)$ is supposed to be an exponentially decaying, interior pressure

$$p_1(t) = p_0 e^{\alpha t} H(t), \tag{1}$$

where p_0 is the amplitude of the pressure, α is the decaying factor, t is the time variable, and $H(t)$ is Heaviside step function, $\alpha = 0$ may represent a sharp change of the pressure perhaps due to a suddenly opening or closing the system.

The impact and separation conditions of the two hollow cylinders are required in the analysis. The initial impact occurs once the dilation of the interior hollow cylinder has first grown to be equal to the value of the clearance. If $u(r, t)$ denotes the radial displacement, the initial impact condition can be written as $u(r, t)|_{r=b_1} - \Delta = 0$, by which the first impact time can be determined. The general impact condition is similar and expressed as equation (2). In equation (2), $\Delta U = u(r, t)|_{r=a_2} - u(r, t)|_{r=b_1}$ is the relative radial displacement of the two interfaces: the inner boundary surface of the outer hollow cylinder and the outer boundary surface of the interior hollow cylinder. A term of $-\Delta$ is added to consider non-zero clearance, which is different from the impact condition in reference [10]. During impacting, the two hollow cylinders are in contact and generate interface impact pressure. At the end of an impact, the interface impact pressure becomes zero and a separation of the two hollow cylinders will start. If $p_2(t)$ denotes the interface impact pressure, the separation condition can be expressed as equation (3), by which the separation time can be determined. Similar impact and separation conditions were applied recently to improve the contact and non-contact criterion in the model of vibration absorbers [12]:

$$\Delta U - \Delta = 0, \qquad \frac{\mathrm{d}(\Delta U)}{\mathrm{d}t} \geqslant 0, \tag{2}$$

$$p_2(r) = 0, \qquad \frac{\mathrm{d}p_2(t)}{\mathrm{d}t} \geqslant 0, \tag{3}$$

During impacting, the interior hollow cylinder is subjected to $p_1(t)$ and $p_2(t)$, and the outer hollow cylinder is subjected to $p_2(t)$. During separating, the interior hollow cylinder is subjected to $p_1(t)$. No force is applied on the outer hollow cylinder, but the inside deformation waves remain propagating. The equations of motion, boundary conditions and initial conditions are expressed as follows:

(1) *In the state before the first impact*:

$$\frac{\partial^2 u(r,t)}{\partial^2 r} + \frac{1}{r}\frac{\partial u(r,t)}{\partial r} - \frac{u(r,t)}{r^2} = \frac{1}{C^2}\frac{\partial^2 u(r,t)}{\partial^2 t}, \quad a_1 \leqslant r \leqslant b_1, \quad t_1 \leqslant t \leqslant t_2^-,$$

$$\sigma_r(r,t)|_{r=a_1} = -p_1(t), \qquad \sigma_r(r,t)|_{r=b_1} = 0,$$

$$u_0(r) = u(r,t)|_{t=t_1} = 0, \qquad v_0(r) = \left.\frac{\partial u(r,t)}{\partial t}\right|_{t=t_1} = 0,$$

$$t_1 = 0, \tag{4a}$$

where the moment of beginning the first impact t_2 is determined by equation (2), t_2^- is the time immediately before t_2, $u_0(r)$ and $v_0(r)$ are the initial radial displacement and radial velocity fields at time t_1 respectively. In this state, the outer hollow cylinder is still at rest.

(2) *In an impact state*:

$$\frac{\partial^2 u(r,t)}{\partial^2 r} + \frac{1}{r}\frac{\partial u(r,t)}{\partial r} - \frac{u(r,t)}{r^2} = \frac{1}{C^2}\frac{\partial^2 u(r,t)}{\partial^2 t}, \quad a_1 \leqslant r \leqslant b_1, \quad t_{2m} \leqslant t \leqslant t_{2m+1}^-,$$

$$\sigma_r(r,t)|_{r=a_1} = -p_1(t), \qquad \sigma_r(r,t)|_{r=b_1} = -p_2(t),$$

$$u_0(r) = u(r,t)|_{t=t_{2m}^-}, \qquad v_0(r) = \left.\frac{\partial u(r,t)}{\partial t}\right|_{t=t_{2m}^-}, \tag{4b}$$

$$\frac{\partial^2 u(r,t)}{\partial^2 r} + \frac{1}{r}\frac{\partial u(r,t)}{\partial r} - \frac{u(r,t)}{r^2} = \frac{1}{C^2}\frac{\partial^2 u(r,t)}{\partial^2 t}, \quad a_2 \leqslant r \leqslant b_2, \quad t_{2m} \leqslant t \leqslant t_{2m+1}^-,$$

$$\sigma_r(r,t)|_{r=a_2} = -p_2(t), \qquad \sigma_r(r,t)|_{r=b_2} = 0.$$

$$u_0(r) = u(r,t)|_{t=t_{2m}^-}, \qquad v_0(r) = \left.\frac{\partial u(r,t)}{\partial t}\right|_{t=t_{2m}^-} \tag{4c}$$

and and additional continuity condition

$$\Delta U = u(r,t)|_{r=a_2} - u(b_1,t)|_{r=b_1} = \Delta, \tag{4d}$$

where m is the number of impacts, $m = 1, 2, \ldots, t_{2m}$ denotes the moment of beginning the mth impact, and the moment of terminating the mth impact or beginning of the mth separation t_{2m+1} is determined by equation (3).

(3) *In a separation state*:

$$\frac{\partial^2 u(r,t)}{\partial^2 r}+\frac{1}{r}\frac{\partial u(r,t)}{\partial r}-\frac{u(r,t)}{r^2}=\frac{1}{C^2}\frac{\partial^2 u(r,t)}{\partial^2 t},\quad a_1\leqslant r\leqslant b_1,\quad t_{2m+1}\leqslant t\leqslant t^-_{2m+2},$$

$$\sigma_r(r,t)|_{r=a_1}=-p_1(t),\qquad \sigma_r(r,t)|_{r=b_1}=0,$$

$$u_0(r)=u(r,t)|_{t=t^-_{2m+1}},\qquad v_0(r)=\left.\frac{\partial u(r,t)}{\partial t}\right|_{t=t^-_{2m+1}},\tag{4e}$$

$$\frac{\partial^2 u(r,t)}{\partial^2 r}+\frac{1}{r}\frac{\partial u(r,t)}{\partial r}-\frac{u(r,t)}{r^2}=\frac{1}{C^2}\frac{\partial^2 u(r,t)}{\partial^2 t},\quad a_2\leqslant r\leqslant b_2,\quad t_{2m+1}\leqslant t\leqslant t^-_{2m+2},$$

$$\sigma_r(r,t)|_{r=a_2}=0,\qquad \sigma_r(r,t)|_{r=b_2}=0,$$

$$u_0(r)=u(r,t)|_{t=t^-_{2m+1}},\qquad v_0(r)=\left.\frac{\partial u(r,t)}{\partial t}\right|_{t=t^-_{2m+1}},\tag{4f}$$

where the moment of beginning the $(m+1)$th impact $t_{2m+2}(t_{2(m+1)})$ is determined by equation (2).

Because the dynamic response of the system is governed by two sets of equations, the exact solutions need to be solved by treating the separation and impact cases separately.

In a separation state, the two hollow cylinders can be considered separately. The solution of a single hollow cylinder subjected to interior and outer pressures can be applied. For a single hollow cylinder with inner radius a and outer radius b, where the inner boundary surface is subjected to an interior pressure $p_1^*(t)$ and the outer boundary surface is subjected to an outer pressure $p_2^*(t)$, the expansion theorem states that the general solution [13–15] can be expressed as

$$u(r,t)=u_s(r,t)+\sum_{m=1}^{N}U_m(r)q_m(t),\tag{5}$$

where the quasi-static radial displacement $u_s(r,t)$ satisfies inhomogeneous boundary conditions, the eigenfunctions $U_m(r)$ satisfy homogeneous boundary conditions, $q_m(t)$ are the unknown time functions, and N represents the number of truncation terms:

$$u_s(r,t)=\left[\frac{a^2}{2(\lambda+\mu)(b^2-a^2)}r+\frac{a^2b^2}{2\mu(b^2-a^2)}\frac{1}{r}\right]p_1^*(t)$$

$$-\left[\frac{b^2}{2(\lambda+\mu)(b^2-a^2)}r+\frac{a^2b^2}{2\mu(b^2-a^2)}\frac{1}{r}\right]p_2^*(t),\tag{6}$$

$$U_m(r) = A_m \varepsilon_1(k_m, r), \tag{7}$$

$$\varepsilon_1(k_m, r) = M_2(k_m, a) J_1(k_m r) - M_1(k_m, a) Y_1(k_m r),$$

$$M_1(k_m, r) = k_m J_1(k_m r) + \frac{\lambda}{\lambda + \mu} \frac{1}{r} J_1(k_m r),$$

$$M_2(k_m, r) = k_m Y_1(k_m r) + \frac{\lambda}{\lambda + \mu} \frac{1}{r} Y_1(k_m r),$$

where k_m is the wave number of order m, $\omega_m = k \cdot C$ is the natural frequency obtained from the frequency equation [10], J_1 and Y_1 are the Bessel functions of the first and second kind of the first order, respectively, and the factor A_m is determined by the normalization condition [13, 10]. It is convenient for considering different separation states by introducing a new time variable t^* to denote the beginning of a separation. Then the improvement of $q_m(t)$ [10] is

$$q_m(t) = q_m(0) \cos \omega_m(t - t^*) + \frac{1}{\omega_m} q_m(0) \sin \omega_m(t - t^*)$$

$$+ \frac{1}{\omega_m} \int_O^{t - t^*} \ddot{Q}_m(t^* + \tau) \sin \omega_m(t - t^* - \tau) \, \mathrm{d}\tau, \tag{8}$$

$$Q_m(t) = -2\pi \int_a^b u_s(r, t) U_m(r) r \, \mathrm{d}r,$$

$$q_m(0) = 2\pi \int_a^b u_0(r) U_m(r) r \, \mathrm{d}r + Q_m(t^*),$$

$$q_m(0) = 2\pi \int_a^b v_0(r) U_m(r) r \, \mathrm{d}r + \dot{Q}_m(t^*).$$

Therefore, from equations (5)–(8), $u(r, t)$ can be expressed as a function

$$u(r, t) = U(r, t, t^*, C, \lambda, \mu, a, b, u_0(r), v_0(r), p_1^*(t), p_2^*(t)) \tag{9}$$

and the radial velocity $v(r, t)$ is

$$v(r, t) = \frac{\partial U}{\partial t}(r, t, t^*, C, \lambda, \mu, a, b, u_0(r), v_0(r), p_1^*(t), p_2^*(t)). \tag{10}$$

Hence, during the state before the first impact, the solution is

$$u(r,t)=\begin{cases}U(r,t,t_1,C,\lambda,\mu,a_1,b_1,0,0,p_1(t),0), & a_1\leqslant r\leqslant b_1,\\ 0, & a_2\leqslant r\leqslant b_2,\\ & t_1\leqslant t\leqslant t_2^-\end{cases}\tag{11}$$

and during the mth separation, the solution is

$$u(r,t)=\begin{cases}U(r,t,t_{2m+1},C,\lambda,\mu,a_1,b_1,u(r,t_{2m+1}^-),v(r,t_{2m+1}^-),p_1(t),0), & a_1\leqslant r\leqslant b_1,\\ U(r,t,t_{2m+1},C,\lambda,\mu,a_2,b_2,u(r,t_{2m+1}^-),v(r,t_{2m+1}^-),0,0), & a_2\leqslant r\leqslant b_2,\end{cases}$$
$$t_{2m+1}\leqslant t\leqslant t_{2m+2}^-,\tag{12}$$

In an impact site, the solutions cannot be obtained directly because of the unknown interface impact pressure $p_2(t)$, but some simplification has been applied in the impact system consisting of two hollow cylinders with zero clearance in our previous work [10]. When two hollow cylinders with zero clearance are in contact, it has been proved that the system has the same natural frequencies and solutions as a single hollow cylinder: an assumed total hollow cylinder with inner radius a_1 and outer radius b_2 subjected to the interior pressure $p_1(t)$. In this paper, if the clearance is much smaller than radius b_1, the simplification can be applied approximately, but the different continuity condition (4d) results in a different solution of $u_s(r,t)$:

$$u_s(r,t)=\begin{cases}(A_{tot}r+B_{tot}r^{-1})p_1(t)+A_{totf}r+B_{tot}r^{-1}, & a_1\leqslant r\leqslant b_1,\\ (C_{tot}r+D_{tot}r^{-1})p_1(t)+C_{totf}r+D_{tot}r^{-1}, & a_2\leqslant r\leqslant b_2,\end{cases}\tag{13}$$

$$A_{tot}=\frac{a_1^2-b_1^2A_s}{2(\lambda+\mu)(b_1^2-a_1^2)},\qquad B_{tot}=\frac{a_1^2b_1^2(1-A_s)}{2\mu(b_1^2-a_1^2)},$$

$$A_{totf}=\frac{-b_1^2B_s}{2(\lambda+\mu)(b_1^2-a_1^2)},\qquad B_{totf}=\frac{-a_1^2b_1^2B_s}{2\mu(b_1^2-a_1^2)},$$

$$C_{tot}=\frac{a_2^2A_s}{2(\lambda+\mu)(b_2^2-a_2^2)},\qquad D_{tot}=\frac{a_2^2b_2^2A_s}{2\mu(b_2^2-a_2^2)},$$

$$C_{totf}=\frac{-a_2^2B_s}{2(\lambda+\mu)(b_2^2-a_2^2)},\qquad D_{totf}=\frac{-a_2^2b_2^2B_s}{2\mu(b_2^2-a_2^2)},$$

$$A_s=\frac{2(a_1^2b_1)/(b_1^2-a_1^2)/((\lambda+2\mu)/(\lambda+\mu)\mu)}{2(a_2)/(b_2^2-a_2^2)/(a_2^2/(\lambda+\mu)+b_2^2/\mu)+(b_1/2(b_1^2-a_1^2)/(a_1^2/(a+\mu)+b_1^2/\mu)},$$

$$B_s=-\frac{\Delta\cdot A_s}{((a_1^2b_1/2(b_1^2-a_1^2))/((\lambda+\mu)/(\lambda+\mu)2\mu))}.$$

Function (9) should be improved by adding the parameter Δ, so as to express $u(r,t)$ in an impact state

$$u(r,t) = U_1(r,t,t^*,C,\lambda,\mu,a,b,\Delta,u_0(r),v_0(r),p_1^*(t),p_2^*(t)). \tag{14}$$

The process of solving function (14) is similar to that of solving function (9). Thus, during the mth impact, the solution is

$$u(r,t) = U_1(r,t,t_{2m},C,\lambda,\mu,a,b,\Delta,u(r,t_{2m}^-),v(r,t_{2m}^-),p_1(t),0),$$

$$a_1 \leqslant r \leqslant b_2, \quad t_{2m} \leqslant t \leqslant t_{2m+1}^- \tag{15}$$

and the interface impact pressure $p_2(t)$ can be obtained readily:

$$p_2(t) = -\sigma_r(r,t)|_{r=b_1} = -\left[(\lambda+\mu)\frac{\partial u(r,t)}{\partial r} + \lambda\frac{u(r,t)}{r}\right]_{r=b_1}, \tag{16}$$

where $\sigma_r(r,t)$ is the radial stress component.

From equations (11), (15) and (12), a sequence of solutions in the time domain can be obtained.

For small clearance, it can be proved easily that $u(r,t)/p_0$ is unchanged with constant Δ/p_0. Hence some equivalent parameters $\Delta_e = \Delta \times 10^{12}/p_0$, $P_{2e}(t) = p_2(t)/p_0$ and $U_e(r,t) = u(r,t) \times 10^{12}/p_0$ are introduced. In this paper, $U_e(r,t)|_{r=b1}$ by $U_{e1}(t)$, and $U_e(r,t)|_{r=a_2}$ by $U_{e2}(t)$ are represented. In addition, if not specified, N and n in terms of time-step length $((b_2 - a_1)/C)/(1/n)$ are 200 and 100 respectively.

3. THE CLUSTERING PHENOMENON

The impact response is related to impacts. In Figure 2, the three curves of $P_{2e}(t)$, $U_{e1}(t) - \Delta$ and $U_{e2}(t)$ show the impact conditions and the relationships between them. The impact response may be periodic (Figure 2(a)) and non-periodic (Figure 2(d)). When apparently continuous impacts as shown in Figure 2(a) take place, the two curves of $U_{el}(t) - \Delta$ and $U_{e2}(t)$ are almost the same and cannot be identified in low-resolution power. The two hollow cylinders behave like one. In other cases, the two interfaces, both the inner boundary surface of the outer hollow cylinder and the outer boundary surface of the interior hollow cylinder may oscillate in either similar or different ways.

More than 100 impacts take place during the considered time interval in each case in Figure 2. They are called multiple impacts [10] to distinguish them from the problem of single impact in the classical impact theory. Impacts may appear continuous (see Figure 2(a)), regular (see Figure 2(b)) and irregular (Figure 2(d)) as the system parameters vary.

The history of $p_2(t)$ in Figure 2(c) illustrates 24 impact clusters. Each impact cluster may consist of several sub-impacts. Figure 3 enlarges the 21st impact cluster

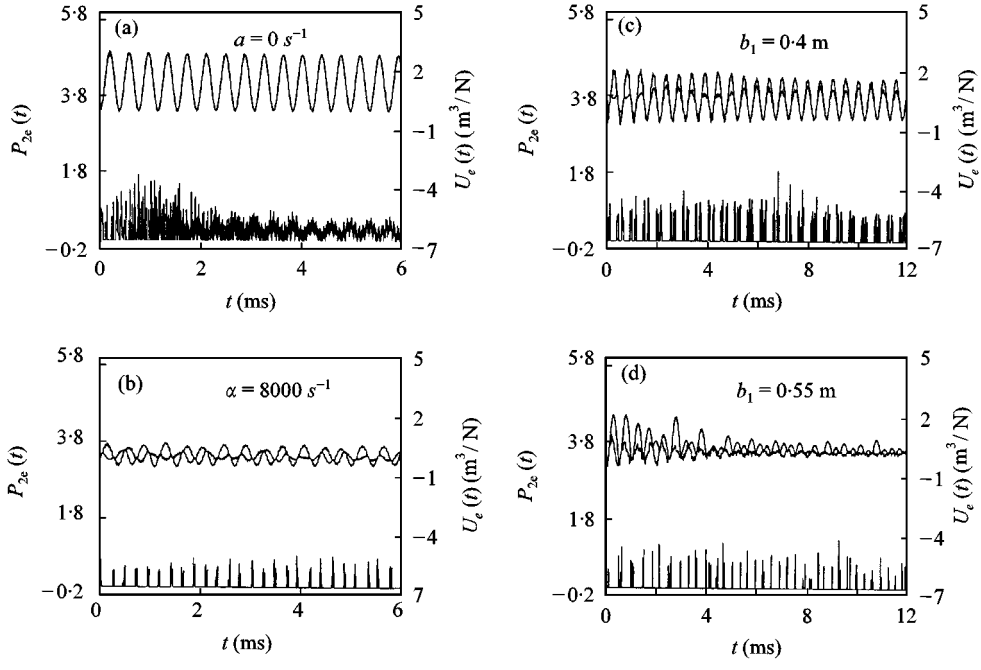

Figure 2. Sample plots of $P_{2e}(t)$ (bottom), $U_{e1}(t) - \Delta$ (middle) and $U_{e2}(t)$ (top): (a) and (b) $a_1 = 0{\cdot}2$ m, $b_1 = 0{\cdot}3$ m, $b_2 = 0{\cdot}4$ m, $\Delta_e = 0$, (c) and (d) $a_1 = 0{\cdot}2$ m, $b_2 = 0{\cdot}6$ m, $\alpha = 0$, $\Delta_e = 0{\cdot}5$ m$^3/N$, $N = 150$.

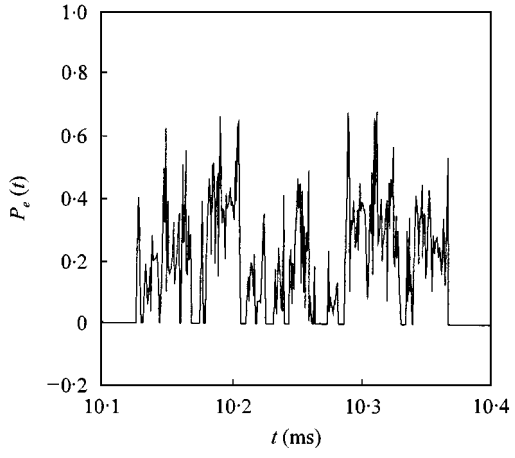

Figure 3. Enlargement of the 21st impact cluster in Figure 2(c).

that consists of 15 sub-impacts. This phenomenon, in which several single impacts take place closely together to form an impact cluster, was called the "group" phenomenon [10]. It may also be called the clustering phenomenon visually. In Figure 2(a), the clusters connect with neighboring clusters, but the impact clusters can be identified. In Figures 2(b), (c), the clustering phenomenon is clear. In Figure 2(d), the clustering phenomenon is unclear, but the impact clusters can also be identified in some time intervals, where some impact clusters may consist of only

one or two single impacts. In Figure 2, the two interfaces seem to oscillate in response to the impact clusters, and not to the single impacts. The clustering phenomenon seems to be an inherent phenomenon in impact systems.

When the clustering phenomenon occurs, the impact cluster may be considered as an output of the system. It has different properties from the single impact. Let N_c denote the number of impact clusters, and N_i denote the number of single impacts. Figure 4 shows an interesting comparison, where N_i varies greatly, but N_c is nearly unchanged with N and n.

Because the time-step length is chosen to be $((b_2 - a_1)/C)/(1/n)$, a larger n can detect shorter and slighter sub-impacts. However, N_i will not approach a constant until a very short time-step length with $n = 500$. In equation (5), each eigenfunction includes a natural frequency considered. For $N = 1$, only the first natural frequency, i.e. the base frequency is considered. The treatment may be very similar to that of a simplified model in which an impact body is represented by a mass attached to a spring. In this case, the solution does not consider the wave effects, and is a vibro-solution. As a larger N is selected and more natural frequencies are considered, one may expect a good detection of sub-impacts. However, the results were unsatisfactory. As shown in Figure 4(b), the values of N_i for $N = 180$ and 200 still have a large difference. It seems to be very different from the numerical results of the dynamics of a single hollow cylinder [14], where $N = 25$ is sufficient. Fortunately, N_c is not so sensitive to n and N. For $N \geqslant 50$ and $n \geqslant 10$, we have checked the time histories of $P_{2e}(t)$, $U_{e1}(t)$ and $U_{e2}(t)$. The variations with N and n are small for steady state responses. This is why $n = 100$ and $N = 200$ are selected in the present paper.

The impact cluster is less sensitive to calculating errors. We may expect that it is also less sensitive to system parameters that to the single impact. It is verified by a comparison between N_c and N_i as shown in Figure 5. N_i varies sharply even on much smaller scales. In Figure 5(a), the two small graphs amplify the small windows

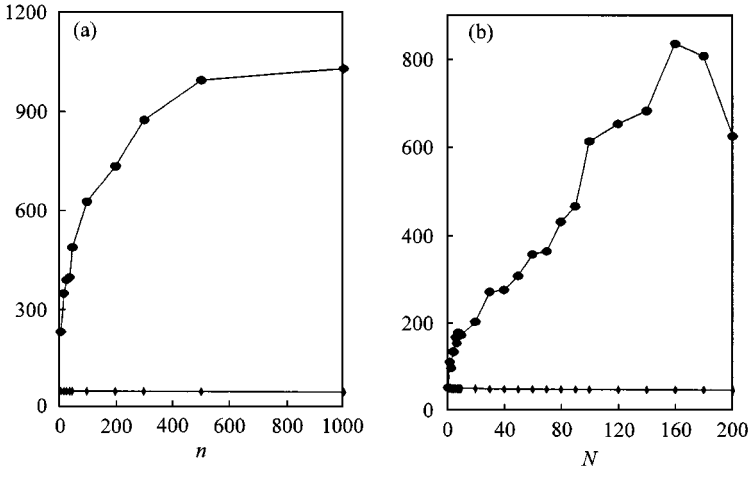

Figure 4. Variations of N_c and N_i: $a_1 = 0{\cdot}2\,\mathrm{m}$, $b_1 = 0{\cdot}4\,\mathrm{m}$, $b_2 = 0{\cdot}6\,\mathrm{m}$, $\alpha = 0$, $\Delta_e = 0{\cdot}5\,\mathrm{m}^3/N$. (a) —●— N_i; —◆— N_c. (b) —●— N_i; —◆— N_c.

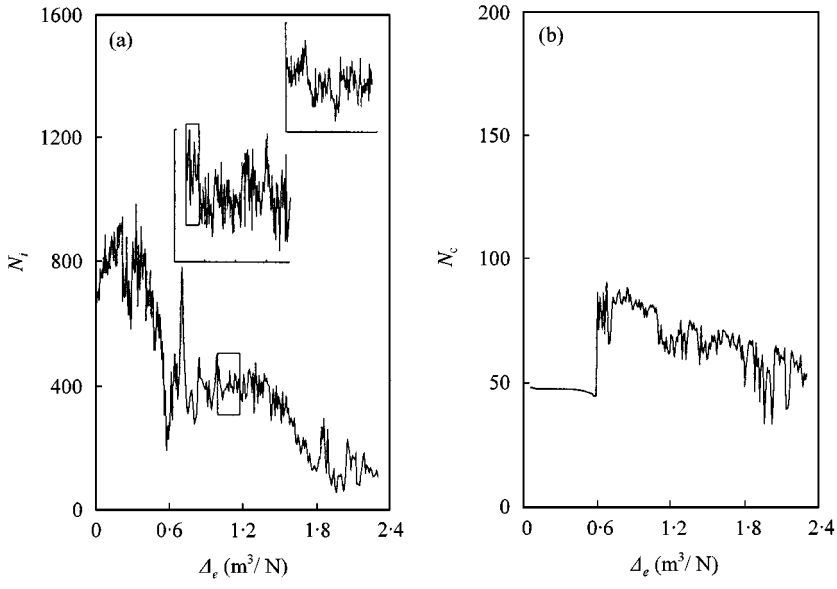

Figure 5. Variations of N_c and N_i with Δ_e: $a_1 = 0.2$ m, $b_1 = 0{\cdot}4$ m, $b_2 = 0{\cdot}6$ m, $\alpha = 0$.

region in the graphs, below which show the variation of N_i to be rather random. A very small difference in the system parameter may cause a sharp variation in N_i. However, N_c has a much lower level of variation as shown in Figure 5(b). It varies slowly before $\Delta_e = 0{\cdot}6\ \text{m}^3/N$, and either slowly or more quickly later on. The difference between $N = 200$ and 50 is examined which is small. A jump at $\Delta_e = 0{\cdot}6\ \text{m}^3/N$ is due to the cluster splitting and the method of counting N_c, which will be discussed later. In more sharply varying regions $\Delta_e = 0{\cdot}6\ \text{m}^3/N \sim 0{\cdot}8\ \text{m}^3/N$ and $\Delta_e = 1{\cdot}8\ \text{m}^3/N \sim 2{\cdot}4\ \text{m}^3/N$, the behaviour of the system will change appreciably. If another system parameter α is changed, the same results can be obtained.

Because the impact cluster and single impact have very different properties, two questions are to be answered: why the impact cluster grows so steadily with n and N, and whether the impact response has the same sensitivity as the impact cluster. As an interpretation of the first question, the time histories of the interface impact pressure for $N = 1, 2$ and 200 are shown in Figure 6. They have similar structures. The structure for $N = 2$ is analogous to that for $N = 200$ even regarding the details. Hence, it is not necessary to detect impact clusters by selecting a larger n and N.

The graphs in Figure 2 may shed some light on the second question, where the two interfaces oscillate perhaps mainly in correspondence with the growth of impact clusters. Being less sensitive to wave effects than stresses, the impact oscillating will have less sensitivity than even the impact cluster. There is no need to vary N and n to check the sensitivity of the steady state response; only checking the unsteady state response will be sufficient. Figure 7 is an example. For $\Delta_e = 1{\cdot}9\ \text{m}^3/N$, the response is chaotic (analyzed in next section). Although the divergence of responses for different N grows and will become large, for $N = 50$, 100 and 200 their spectra are similar. The essential features of the impact system in the frequency domain hardly change with small calculating errors.

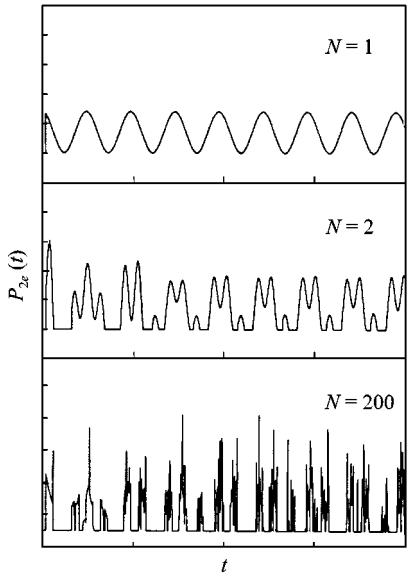

Figure 6. Graphs of $P_{2e}(t)$ when $N = 1$, 2 and 200: $a_1 = 0{\cdot}2\,\text{m}$, $b_1 = 0{\cdot}4\,\text{m}$, $b_2 = 0{\cdot}6\,\text{m}$, $\alpha = 0$, $\Delta_e = 0{\cdot}1\,\text{m}^3/\text{N}$.

Moreover, by comparing the level of white noise in Figure 7, a criterion of selecting N may be obtained. A white noise occurs after a frequency of 3000/s when $N = 50$ and 100. It occurs in reality throughout the frequency domain, but does not occur when $N = 200$. Hence, the measurement of the level of white noise caused by the truncation error may serve as a criterion to select N.

In the simplified models, an impacting body is usually modelled as a mass attached to a spring. Only the base frequency mode is considered. The treatment of choosing $N = 1$ in equation (5) for the present impact system is similar to that of the simplified models. In Figure 6, the similar structures of $P_{2e}(t)$ for $N = 1$, 2 and 200 may show some validity of the simplified models. The main reason for the validity of the simplified models is that the base frequency usually occupies most parts of the energy of oscillations. In this case, the base frequency dominates the main impact clusters, the clustering phenomenon may occur and the simplified models may be somewhat valid in uncovering the essential features of the impact system.

The occurrence of the clustering phenomenon should be related to the quasi-static behavior of the impact system. According to the impact condition, the relative radial displacement of the two interfaces dominates the generation of impacts. The impact cluster and response interact with each other and cause complicated motions. Figure 6 shows that the oscillation at the base frequency dominates the profile of the impact cluster, and the oscillations at higher frequencies dominate sub-impacts. The occurrence of the clustering phenomenon is related to the wave effects because impacts usually accompanying the wave phenomenon. When the changes of the oscillations due to waves are smaller than the general levels of oscillations, the system behaves quasi-statically. The additional sub-impacts generated by high-frequency oscillations will concentrate on some

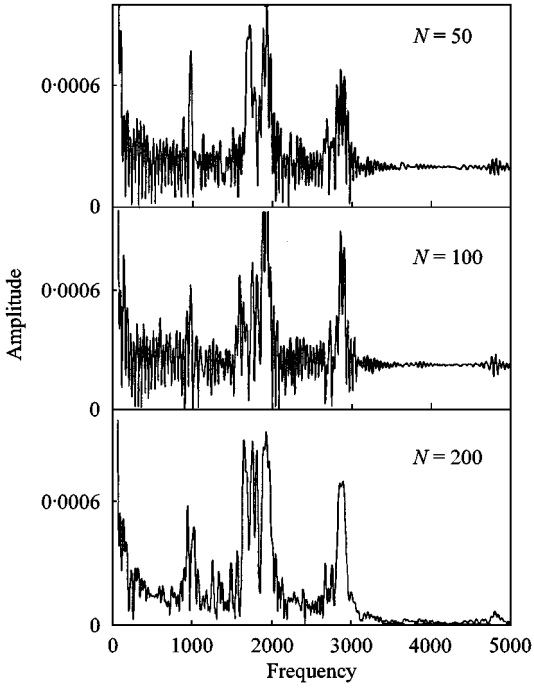

Figure 7. Frequency spectra: $a_1 = 0{\cdot}2\,\text{m}$, $b_1 = 0{\cdot}4\,\text{m}$, $b_2 = 0{\cdot}6\,\text{m}$, $\alpha = 0$, $\Delta_e = 0{\cdot}1\,\text{m}^3/N$.

time intervals that are dominated by the base frequency, and form the impact clusters as shown in Figure 6 when when $N = 200$. The clustering phenomenon will occur clearly. In this case, the simplified models may have some validity. In Figure 6, $N = 1$ may represent a simplified model with more degrees of freedom. One might note that in Figure 2 the clustering phenomenon is clear if the two interfaces oscillate quasi-statically.

If the changes of the oscillation due to the waves are considerable in comparison to the general levels of oscillations, high frequencies with more energy are excited. The system does not behave quasi-statically. More sub-impacts splitting from the main impact clusters will fill the left time intervals more irregularly as shown in Figure 2(d). Then the clustering phenomenon is unclear.

However, when the simplified model is applied, it is necessary to choose as many more degrees of freedom as possible. An improvement of the impact law with zero contact time should also be made. Otherwise the model will fail to apply to the case even for the continuous impacts as shown in Figure 2(a).

Because the impact response depends on the impact cluster, it will depend on the evolution of the impact cluster. Two evolving ways have been found: splitting and discontinuous bifurcation. Figure 2 gives us the insight to discover the evolving way of splitting. As the parameters increase, the impact clusters are thinned and then split into sub-clusters (usually split into two sub-clusters first). Comparing the distributions of $P_{2e}(t)$ between $N = 2$ and 200 in Figure 6, the splitting is due to high natural frequencies. Two main sub-clusters are mainly due to the second natural frequency. The splitting is unavoidable.

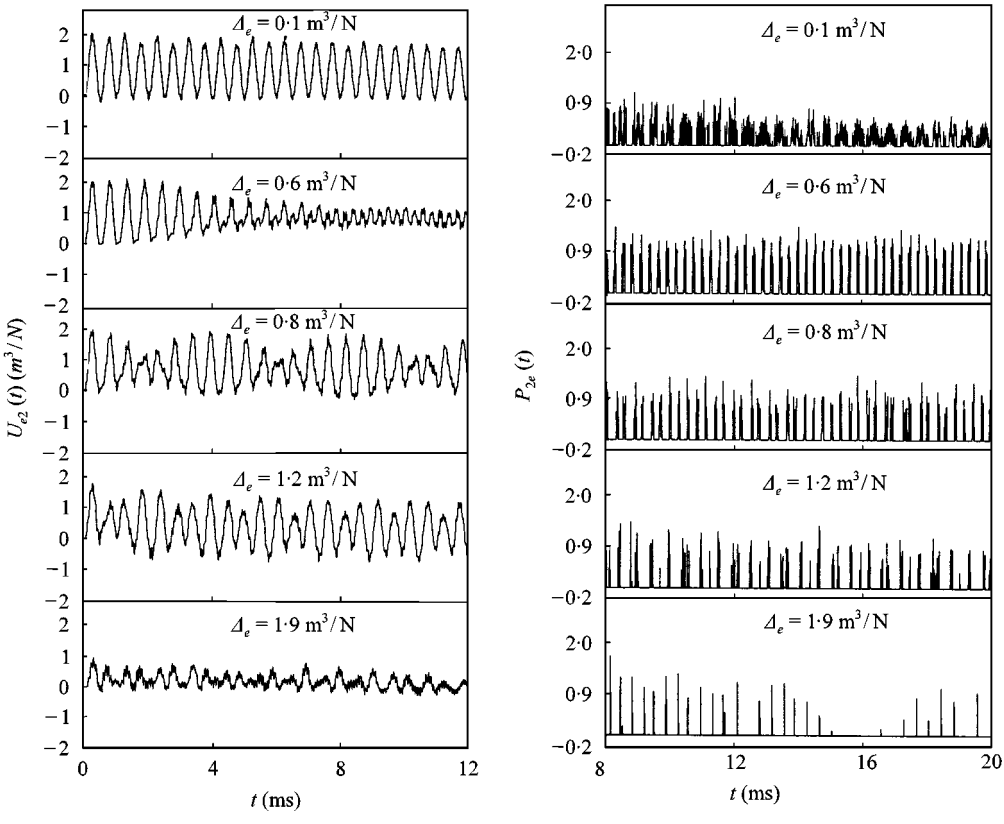

Figure 8. Evolution of the impact cluster and response: $a_1 = 0{\cdot}2$ m, $b_1 = 0{\cdot}4$ m, $b_2 = 0{\cdot}6$ m, $\alpha = 0$.

The splitting way may be subtle. In the system with the parameters given in Figures 5 and 8, the splitting takes place early, but when near $\Delta_e = 0{\cdot}6\ \mathrm{m}^3/N$, the hyper-harmonic oscillation becomes strong. Sub-clusters are counted only after $\Delta_e = 0{\cdot}6\ \mathrm{m}^3/N$, so that a jump in Figure 5(b) occurs. As the system evolves, the number of single impacts in an impact cluster decreases. The impact cluster becomes more sensitive. When the impact cluster comprises only one or two single impacts, for instance, at $\Delta_e = 1{\cdot}9\ \mathrm{m}^3/N$, it will be as sensitive as the single impact. This is why N_c varies sharply after $\Delta_e = 0{\cdot}6\ \mathrm{m}^3/N$ and becomes almost the same as N_i after $\Delta_e = 1{\cdot}8\ \mathrm{m}^3/N$.

Figure 8 also shows the discontinuous evolution. Initially, impact clusters become thinner and then some clusters begin to vanish. The discontinuity may occur suddenly. This evolving way usually accompanies the splitting of clusters. The evolution of the impact cluster is the precursor of the evolution of the system.

4. NON-LINEAR IMPACT RESPONSE

To consider multiple sub-impacts, the impact response is investigated by the use of the continuous model and theory of wave propagation. The system is described

by a partial differential (equation (4)) whose phase space is infinite dimension. Hundreds of impacts take place within the considering time intervals. The applied force $p_1(t)$ is a continuously non-period load. Under these conditions, the impact response of the system is more complicated. Even for the apparently regular response as in Figure 8 at $\Delta_e = 0{\cdot}1\ \mathrm{m}^3/N$, the phase portrait (displacement–velocity) is complicated and random looking (see Figure 9). In contrast to the present treatment, the simplified models have a well-defined finite number of degrees of freedom and have shown periodic, non-periodic and low-dimensional chaotic motions [1–5].

In this paper, the evolution of the system will be investigated by observing the time history of oscillation, the frequency spectrum, and the phase portrait in reconstructed phase space. The system parameters: $a_1 = 0{\cdot}2$ m, $b_1 = 0{\cdot}4$ m, $b_2 = 0{\cdot}6$ m, $\alpha = 0$, are chosen, and the clearance Δ_e is varied. The time history of $U_{e2}(t)$ and $P_{2e}(t)$ are shown in Figure 8. The impact clusters evolve in a combined way of splitting and discontinuity. The clustering phenomenon is clear.

Some of the frequency spectra are selected and shown in Figure 10. A route of two-frequency quasi-periodicity to chaos is found. The basic path is periodic $\rightarrow$ quasi-periodic $\rightarrow$ chaotic. It is very similar to the experimental observation in reference [16]. Phase locking is also observed. The observations are described in detail by numerical experiments as follows.

Before $\Delta_e = 0{\cdot}5\ \mathrm{m}^3/N$, a spectral peak appears at a frequency labeled f_1. It is a periodic state with a single spectral peak (Figure 10(a)) and its harmonics (Figure 8). The decaying spectral curve at the beginning is due to quasi-static radial displacement $u_s(r, t)$.

At $\Delta_e = 0{\cdot}5\ \mathrm{m}^3/N$, a doubling frequency $2f_1$ appears. It is clearer at $\Delta_e = 0{\cdot}6\ \mathrm{m}^3/N$ (Figure 10(b)). It is another basic frequency labelled f_2. The spectrum of $\Delta_e = 0{\cdot}6\ \mathrm{m}^3/N$ demonstrates a precursor of a line combination of two basic frequencies in the form $f_3 = f_2 - f_1$. Then the quasi-periodic state with two

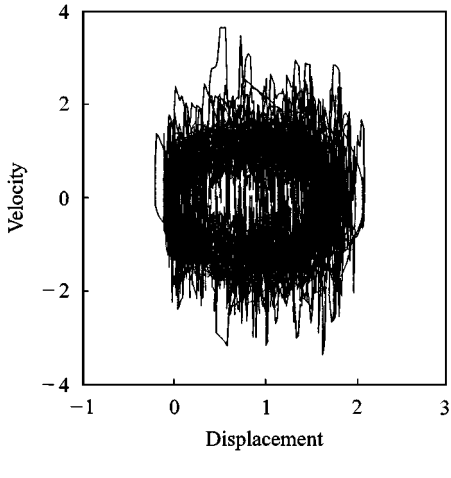

Figure 9. Phase portrait: $a_1 = 0{\cdot}2$ m, $b_1 = 0{\cdot}4$ m, $b_2 = 0{\cdot}6$ m, $\alpha = 0$, $\Delta_e = 0{\cdot}1\ \mathrm{m}^3/N$.

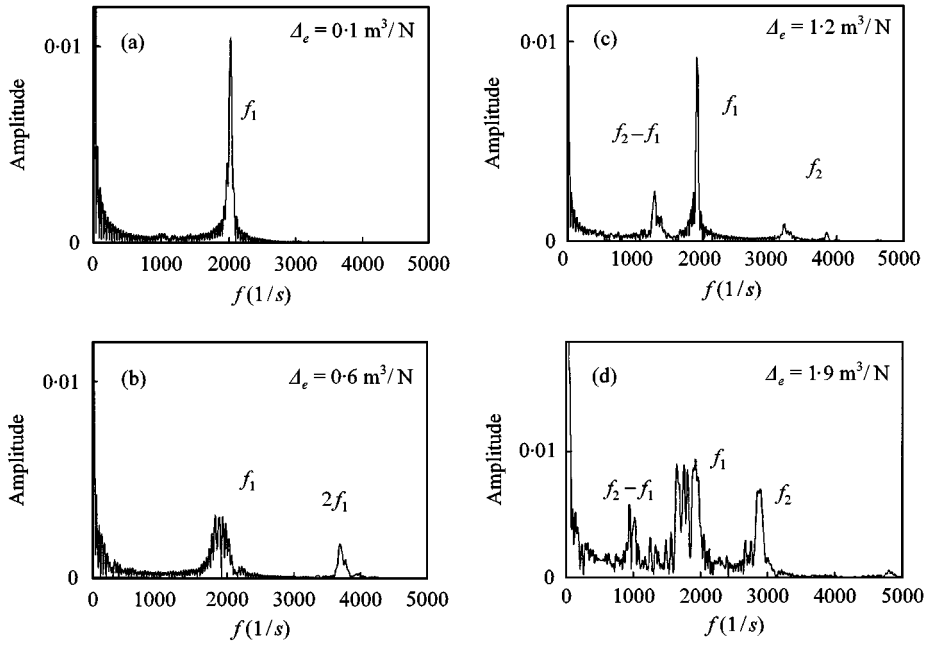

Figure 10. Frequency spectra.

incommensurate frequencies f_1 and f_2 appears. f_3 can be found just splitting from f_1. As Δ_e increases, the separation of f_3 from f_1 increases and the amplitudes of f_1 and f_2 decreases. Other linear combinations can also occur, such as $f_1 + f_2, f_1 + 2f_2, 2f_2$ and $3f_2$, but their peaks are very low. The ratio f_2/f_1 decreases smoothly from 2 to a step $\frac{8}{5}$ as Δ_e increases. The step is reached at $\Delta_e = 1{\cdot}5\ m^3/N$, but a spectral peak at a frequency $f_L = f_2/8 = f_1/5$ does not occur. The phase locking and the linear combination of two basic frequencies f_1 and f_2 show strongly non-linear characterization in the system.

At $\Delta_e = 1{\cdot}9\ m^3/N$, continuous range of frequencies appears, indicating non-periodic motion.

For small clearances, the two hollow cylinders behave like one. For larger clearances, very few impacts take place and the two hollow cylinder eventually oscillate periodically but at their own natural frequencies. Between these two extreme states the two hollow cylinders interact in a strongly non-linear way.

The transition from two-frequency quasi-periodicity o chaos is less understood [17], but it is desirable to find out at least the origins of f_1 and f_2.

Three base frequencies for the analysis are suggested. They are $f_o = 1523$ Hz for the outer hollow cylinder, $f_1 = 2609$ Hz for the interior hollow cylinder, and $f_T = 2052$ Hz for the assumed total hollow cylinder. f_1 approaches f_T as Δ_e decreases, but seems to be never equal to f_T. A difference exists even at $\Delta_e = 0$ when the continuous impacts occur. The reason is that the two interfaces cannot bear the tensile stress. f_1 approaches f_o as Δ_e increases. If only a single impact takes place, f_1 will be equal to f_o. It is observed that in reality f_1 is located between two base frequencies f_T and f_o.

The linewidth of the spectral peak of f_1 is about 280 Hz (5·7 per cent of f_1) at $\Delta_e = 0{\cdot}1\ \mathrm{m}^3/N$. It is so wide that the spectrum looks like a continuous spectrum plotted on a logarithmic vertical scale.

If the frequency spectrum of a single hollow cylinder is calculated, such as the assumed total hollow cylinder subjected to $p_1(t)$, three sharp peaks at the first three natural frequencies can be observed, where the ratio, first peak value/second peak value, is about 1/3. A sharp peak appears at a frequency 12 745 Hz (not shown) in the present system, due to the second natural frequency 12 739 Hz of the assumed total hollow cylinder. This frequency is unchanged with the clearance, but its peak value is very small. It is about 5·6% of the first peak of $f_1 = 1981$ Hz at $\Delta_e = 0{\cdot}6\ \mathrm{m}^3/N$. The impacts seem to force the impact system to be in response to lower frequencies among which more energy is distributed.

One might note that in Figure 8, the sub-clusters split from main impact clusters at $\Delta_e = 0{\cdot}6\ \mathrm{m}^3/N$, and are distributed uniformly within a long time interval. The spectral peak of f_2 is visible. It is 3869 Hz, while f_1 is 1981 Hz. f_2 is just the double of f_1. Its peak is even higher than that of f_1 for the interface of the interior hollow cylinder. The spectra of the interface of the interior hollow cylinder (not shown) demonstrate that f_2 evolves from f_1.

The beginning of f_2 perhaps is related to the splitting of impact clusters, while the splitting is due to higher frequency models as shown in Figure 6. The simplified model, representing an impact body by a mass and a linear spring, will fail to detect this splitting and find the route of two-frequency quasi-periodicity to chaos.

It is known that the interface of the outer hollow cylinder will eventually oscillate periodically as Δ_e increases. If the situation is reversed, a new route to chaos, intermittency, is observed. Figure 11 shows a transition to chaos through

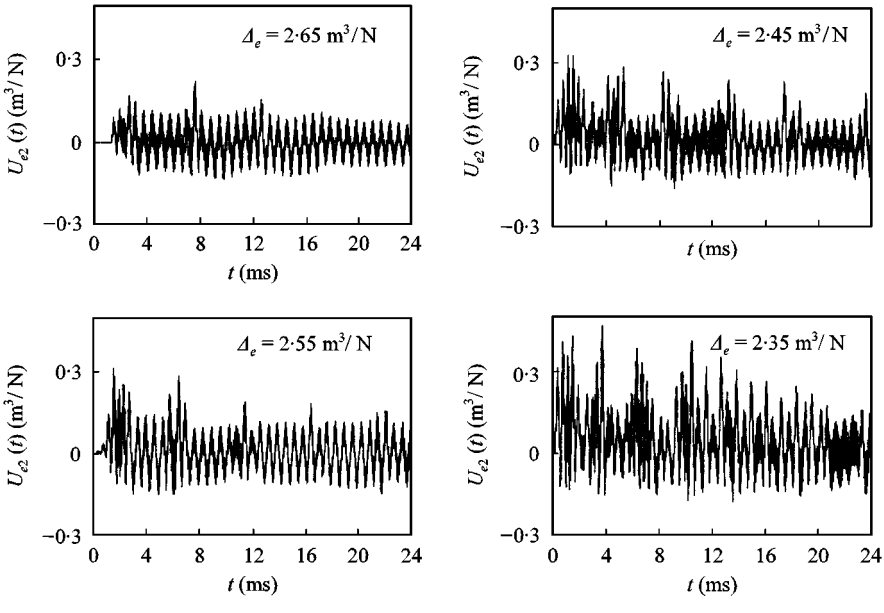

Figure 11. Presence of intermittency.

intermittency. After the clearance is changed near 2·725 m^3/N, more regular periodic oscillations are interrupted abruptly by bursts. As the clearance decreases, the bursts occur more frequently, and the behavior becomes more chaotic.

According to the time series, Fourier spectra and routes to chaos, the present impact system behaves like a low-dimensional system. A few of the low frequencies are excited. It means a few degrees of freedom perhaps can describe the system. To further verify this idea, the phase space of the system is reconstructed from the observable $U_{e2}(t)$. Choosing a 3-D embedding space and the delay time $\tau = 0{\cdot}0864$ ms, three co-ordinates are $W_1 = U_{e2}(t)$, $W_2 = U_{e2}(t + \tau)$ and $W_3 = U_{e2}(t + 2\tau)$. Figure 12 shows the presence of the reconstructed attractors.

Figure 12(a) is a period looking trajectory. After a rotation, a narrow band is shown in Figure 13(a). The trajectory rotating around the torus is due to the existence of another higher frequency 12 745 Hz. As the clearance exceeds 0·5 m^3/N, the torus begins to deform and warp, but the period looking trajectory exists till $\Delta_e = 0{\cdot}599$ m^3/N. After $\Delta_e = 0{\cdot}6$ m^3/N, more complicated trajectories appear as shown in Figure 12(b)–(d). By rotating axes, Figure 13 shows that the bands widen with the clearance. However, these bands which are not so broad show that the low-dimensional attractors may describe the system.

The existence of the low-dimensional attractors is supported by the computation of information dimension D_I (see Figure 14). D_I is computed by using 300 000 points. Before $\Delta_e = 1{\cdot}0$ m^3/N, D_I is about 2·0 and in agreement with the trajectory

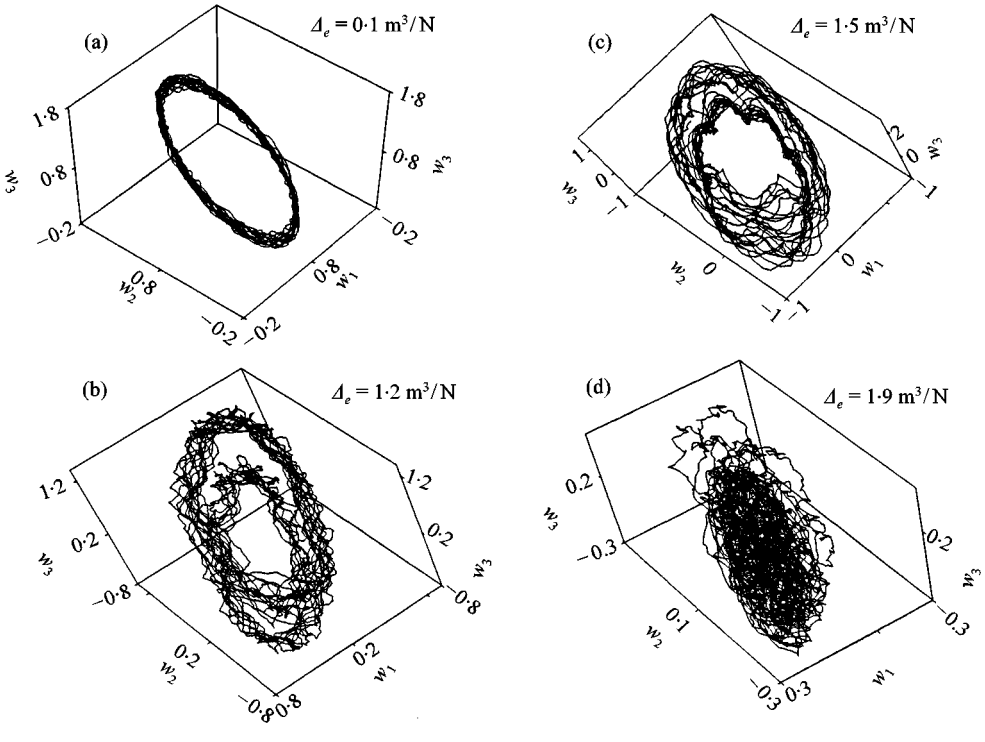

Figure 12. Phase portrait in a 3-D embedding space.

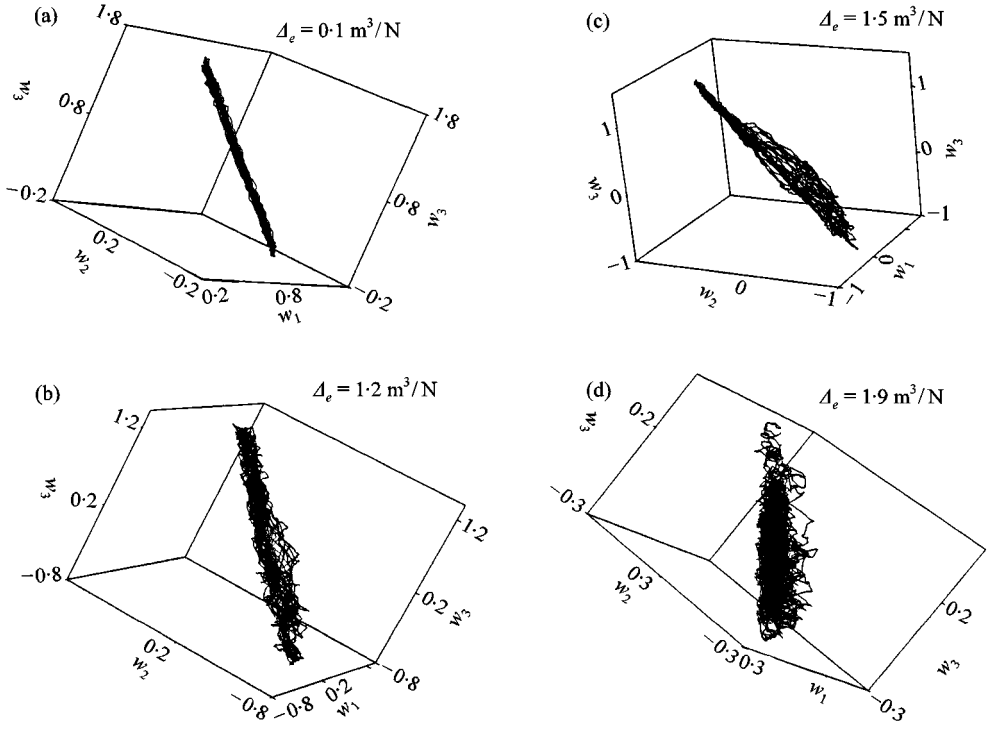

Figure 13. Phase portrait after a rotation.

rotating around a torus. Then the fractal dimension may show the presence of a strange attractor and low-dimensional chaotic motions.

5. CONCLUSIONS AND DISCUSSIONS

Although the multiple-impact phenomenon, complicated motions and routes to chaos discussed in the preceding sections are incomplete and not fully understood, some conclusions from the analysis can be drawn.

The clustering phenomenon is an important feature of impact systems. Whether it occurs is directly related to the validity of the simplified models describing the impact systems. The wave and quasi-static effects may determine if the clustering phenomenon occurs. Because the main energy is usually distributed to the base frequency of the oscillation of a structure, the clustering phenomenon seems to be an inherent physical phenomenon. More stable impact clusters than single impacts hold out a hope for the use of the simplified models. However, if a simplified model is applied, there are many more degrees of freedom to be selected, and the impact laws such as the Hertzian impact law instead of the classical impact law are used with a non-zero contact time.

The calculation of the interface impact pressure allows us to uncover some underlying rules. The evolution of impact clusters is connected to the evolution of the impact system. Two evolving ways of impact clusters, splitting and discontinuity bifurcation, are found. Two evolving ways of the system, from

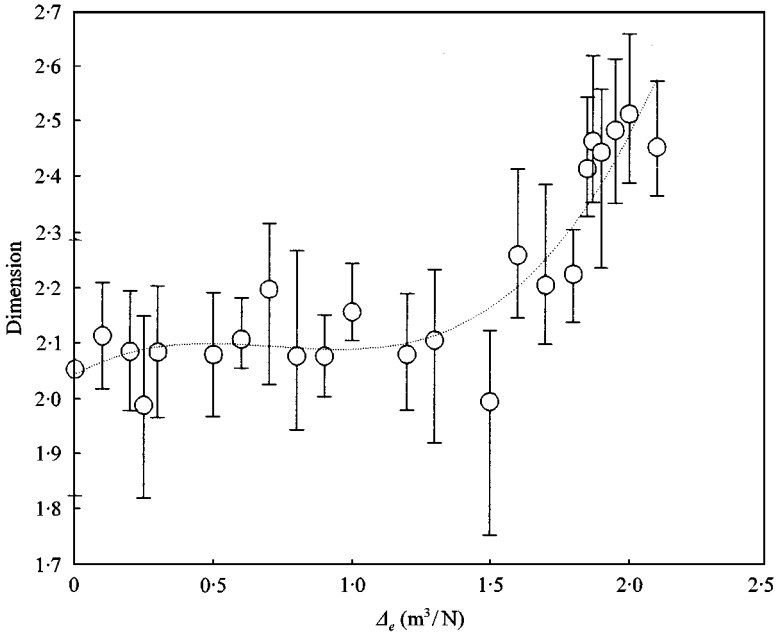

Figure 14. Information dimension versus clearance.

two-frequency quasi-periodicity and through the intermittency to chaos, are observed. They may be two usual ways of the impact systems. Many complicated motions, such as periodic, quasi-periodic, chaotic motions, etc. are observed. The linear combination of two basic frequencies and phase locking are observed as well. The time histories, frequency spectra, phase portraits in reconstructed phase space and information dimension, show the system may exhibit the low-dimensional behavior. The simplified models may be somewhat valid in describing the essential non-linear features of impact systems.

The present study indicates the importance of multiple impacts on impact system, but is incomplete. Further studies are required to be done for the chaotic dynamics of the impact systems.

REFERENCES

1. R. P. S. Han, A. C. J. Luo and W. Deng 1995 *Journal of Sound and Vibration* **181**, 231–250. Chaotic motion of a horizontal impact pair.
2. C. Budd, F. Dux and A. Cliffe 1995 *Journal of Sound and Vibration* **184**, 475–502. The effect of frequency and clearance vibrations on single-degree-of-freedom impact oscillators.
3. S. W. Shaw and P. J. Holmes 1983 *Physical Review Letters* **51**, 623–626. A periodically forced linear oscillator with impacts: Chaos and long period motions.
4. G. S. Wibston 1987 *Journal of Sound and Vibration* **118**, 395–429. Global dynamics of a vibro-impacting linear oscillator.
5. J. M. T. Thompson 1983 *Proceedings of the Royal Society of London A* **387**, 407–427. Complex dynamics of compliant offshore structures.

6. H. L. Masson 1935 *ASME* **58**, A55-A61. Impact of beams.
7. D. Stoianovici and Y. Hurmuzlu 1996 *Journal of Applied Mechanics* **63**, 307–316. A critical study of the applicability of rigid-body collision theory.
8. W. Goldsmith 1960 *Impact*. London, U.K: Edward Arnold Publishers Ltd.
9. A. S. Yigit, A. G. Ulsoy and R. A. Scott 1990 *Journal of Vibration and Acoustics* **112**, 65–70. Dynamics of radially rotating beam with impact, Part 1: theoretical and computational model.
10. X. C. Yin 1997 *International Journal of Solids and Structures* **34**, 4597–4616. Multiple impacts of two concentric hollow cylinders with zero clearance.
11. C. Wang and J. Kim 1996 *Journal of Sound and Vibration* **191**, 809–823. New analysis method for a thin beam impacting against a stop based on the full continuous model.
12. H. Luo and S. Hanagud 1998 *Journal of Applied Mechanics* **65**, 223–233. On the dynamics of vibration absorbers with motion-limiting stops.
13. A. C. Eringen and E. S. Suhubi 1975 *Elastodynamics*, *Vol. 2. Linear Theory*. New York: Academic Press.
14. Y. N. Gong and X. Wang 1991 *Structural Dynamics*: *Recent Advances* (Petyt et al., editor) England: Elsevier Science Publication Ltd. Radial vibration and dynamic stresses in elastic hollow cylinder.
15. X. Wang and Y. N. Gong 1991 *Acta Mechanica Sinca* **7**, 275–285. A theoretical solution for axially symmetric problems in elastodynamics.
16. J. P. Gollub and S. V. Benson 1980 *Journal of Fluid Mechanics* **100**, 449–470. Many routes to turbulent convection.
17. A. A. Tsonis 1992 *Chaos*: *for Theory to Application.* New York: Plenum Press.